Metallogels: a novel approach for the nanostructuration of single-chain magnets

Felix Houard, Guiseppe Cucinotta, Thierry Guizouarn, Yan Suffren, Guillaume Calvez, Carole Daiguebonne, Olivier Guillou, Franck Artzner, Matteo Mannini, Kevin Bernot

ARTICLE

Metallogels: a novel approach for the nanostructuration of single-chain magnets

conReceived 00th January 20xx,
Accepted 00th January 20xx

DOI: 10.1039/x0xx00000x

Felix Houard,[a] Guiseppe Cucinotta,[b] Thierry Guizouarn,[a] Yan Suffren,[a] Guillaume Calvez,[a] Carole Daiguebonne,[a] Olivier Guillou,[a] Franck Artzner,[c] Matteo Mannini*[b] and Kevin Bernot*[ad]

In this study we demonstrate that single-chain magnets (SCMs) can be assembled in gel phase and transferred intact on surface. We take advantage of a family of SCMs based on Tb^{III} ions and nitronyl-nitroxides radicals functionalized with short alkyl chains known to form crystalline supramolecular nanotubes interacting with heptane acting as crystallizing solvent. When the radicals are functionalized with long aliphatic chains a robust gel is formed with similar structural and functional properties respect to its crystalline parent. Indeed, a small-angle X-ray scattering (SAXS) study unambiguously demonstrates that the gel is made of supramolecular nanotubes: the high stability of the gel allows the determination from SAXS data of precise nanotube metrics such as diameter, helical pitch and monoclinic cell of the folded 2D crystal lattice along the tube direction. Additionally, static and dynamic magnetic investigations show the persistence of the SCM behavior in the metallogel. Last, on-surface gelation provides thick films as well as sub-monolayer deposits of supramolecular nanotubes on surface as evidenced by atomic force microscopy (AFM) observations. This paves the road toward magnetic materials and devices made of SCMs profiting of their isolation on surface as individual chains.

Introduction

The design of molecular magnetic materials[1] is one of the strategies to cope with the increasing demand for high-density and energy-efficient data storage devices. Indeed, the amount of data stored each year increases exponentially[2] and traditional top-down approaches will soon face physical limitations.[3] Single-molecule magnets[4] (SMMs) are particularly promising for magnetic data storage[5,6] because they show magnetic bistability of molecular origin[7] thus, in principle, suitable to be used as magnetic memories through a bottom-up approach.[8]

However, the formation of stable magnetic deposits out of these molecules is extremely demanding[9,10] and requires to use of well-protected chemical structures[11,12] or to carefully decouple the molecular layer from metallic surfaces[13] as they can lose or severely lower their ability to store magnetic information when deposited on surfaces. Last, most of the high-performance SMMs[14,15] are extremely air and moisture sensitive and are difficult to handle in a surface deposition process. Crucially, their magnetic behavior is often affected by thermally-independent relaxation mechanisms such as quantum tunneling of the magnetization (QTM)[16] that severely degrade the memorization capabilities in zero field. 1D analogs of SMMs, namely single-chain magnets (SCMs)[17] have greater potential with respect to coordicSMMs. Their magnetic relaxation is not governed by spin-phonon interaction and extended Orbach dynamics as SMMs but by 1D magnetic dynamics[18] that rely on the onset of spin correlation at low temperature thus resulting mostly unaffected by QTM or other thermally independent phenomena.

One of the most studied classes of single-chain magnets is based on nitronyl-nitroxide (NIT) radicals acting as bridging units between 3*d* or 4*f* anisotropic ions (M) forming a molecular chain (Fig. 1) with general formula $(M\text{-}NIT)_\infty$.[19] NIT structure ensures both a good in-chain magnetic interaction via the delocalized radical and an efficient magnetic insulation of each chain via their substituting organic groups.[20] Accordingly, SCM behavior can be observed.[21] SCMs as most of 1D coordination polymers have very low processability because of their very limited stability in vapor phase or in solution (contrary to their building blocks). These facts justify the limited evidence of successful depositions of similar objects on surfaces.[22] Drop casting, step-by-step vertical growth, surface pre-organization, or controlled nanometrization of the chains' crystal[23] have been tested but none of these approaches provided convincing SCM deposits so far through on-surface crystallization studies.[24]

We recently reported the synthesis and the structural characterization of a novel Tb-based SCM derivative (TbC_6 crystal) based on nitronyl-nitroxide ligands functionalized with hexyl chains (2-(4'-(hexyloxy)phenyl)-4,4,5,5-tetramethyl imidazolin-1-oxyl-3-oxide radical, or $NITPhOC_6$) leading to

[a] Univ Rennes, INSA Rennes, CNRS, ISCR (Institut des Sciences Chimiques de Rennes), UMR 6226, Université de Rennes 1, F-35000 Rennes, France. E-mail: kevin.bernot@insa-rennes.fr
[b] Dipartimento di Chimica "Ugo Schiff" (DICUS), Università degli Studi di Firenze, INSTM Research Unit of Firenze, Via della Lastruccia n.3-13, 50019 Sesto Fiorentino (FI), Italy. E-mail: matteo.mannini@unifi.it
[c] CNRS, IPR (Institut de Physique de Rennes), UMR 6251, Université de Rennes 1, F-35000 Rennes, France.
[d] Institut Universitaire de France, 1 rue Descartes, 75005, Paris, France.
†Electronic Supplementary Information (ESI) available. See DOI: 10.1039/x0xx00000x

ARTICLE

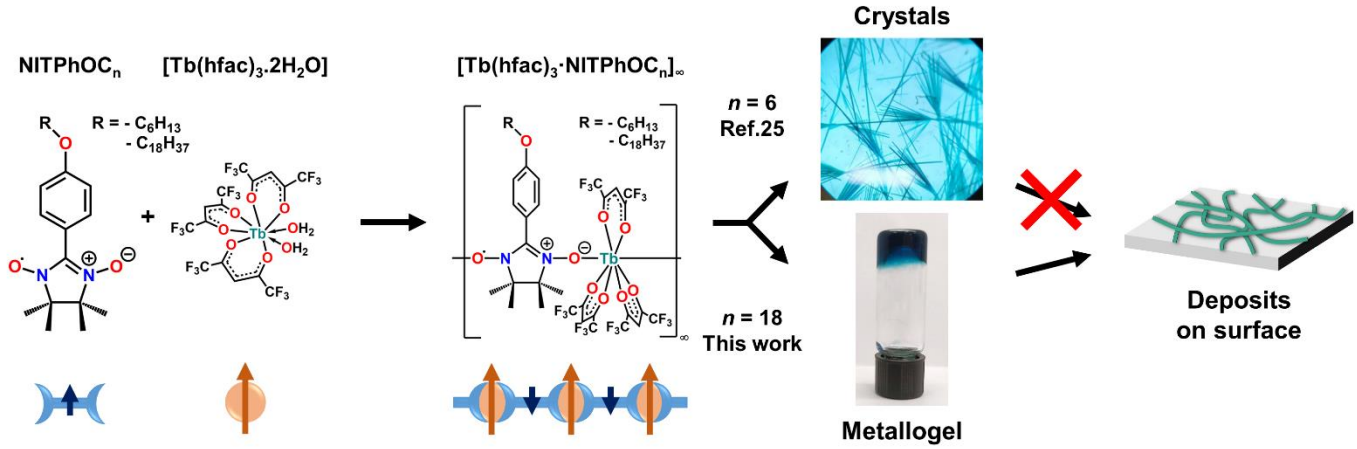

Fig. 1 Schematic chemical strategy adopted in this study.

an unusual crystalline arrangement in the solid phase while preserving their molecular-based magnetic properties.[25] Usually, (M-NIT) units alternate with symmetry-related consecutive angles, and chains have often a zigzag topology that weakly interacts from the supramolecular point of view. The TbC_6 structure features significant structural flexibility via 1) the 4*f* β-diketonate coordination, that provide less directional binding than the 3*d* ones; 2) the presence of a hexyl aliphatic tail as substituent in the para-position of an aromatic NIT: its large degrees of freedom can accommodate various molecular organizations; 3) the interplay of the organic radical alkyl chains with the aliphatic solvent. Indeed, the use of aliphatic solvent promotes weak supramolecular interchain interactions strong enough to generate nanotubes of 4.6 nm diameter made of 11 woven chains, an asset for their deposition on surface because more rigid than isolated ones. However, no progress was made as far as processability is targeted: the TbC_6 molecular chain is destroyed upon solubilization and the supramolecular nanotubes are only stable under their crystalline form. This is a severe drawback to turning these molecules into molecular materials or devices. In particular, they cannot handle surface deposition processes.

This is the reason why we explored a soft matter route for the stabilization of SCM out from the solid phase that consists in forming metallogels of these chains furthermore allowing their deposition on surface (Fig. 1). Metallogels[26–28] are biphasic systems behaving as a thixotropic material preserving most of the properties of their constituents such as the optical, magnetic or redox properties of the eventually embedded metal complexes[29] and gaining some extra features respect to the latter in terms of processability,[30] mechanical robustness and tunability under thermal, photo, magnetic or mechanic stimuli.[31–33] Accordingly, they are an efficient intermediate toward molecule-based functional devices.[34–36] Metallogels have been obtained either with supramolecular compounds,[31,37–40] metal-organic frameworks,[41] spin-crossover molecules,[42–45] magnetically coupled radicals[46] or 3*d* ions.[47] Here, we demonstrate that starting from a long chain NIT derivative, it is possible to promote the formation of a metallogel enhancing the processability of the SCM and allowing their deposition on surfaces to pave the road to the development of magnetic materials and devices based on functional properties of SCMs.

Results and discussion

Synthesis and gelation properties

A nitronyl nitroxide radical bearing a long octadecyl alkyl chain has been designed to promote the formation of an SCM system with a metallogel behavior. That radical of formula $NITPhOC_{18}$ (where $NITPhOC_{18}$ = 2-(4'-(octadecyloxy)phenyl)-4,4,5,5-tetramethylimidazolin-1-oxyl-3-oxide) has been synthesized following the Ullman procedure[48] (Fig. S1) and crystallized as thin blue plates (Fig. S2, Table S1). Once reacted with $Tb(hfac)_3{\cdot}2H_2O$ ($hfac^-$ = hexafluoroacetylacetonate) the solution was cooled down and the solvent was removed under reduced pressure, allowing the solution to evaporate gradually and turn from blue to cyan until the complete drying, giving a dark amorphous latex-like solid called TbC_{18} precursor (see Fig. 2). This color change, already reported for similar crystalline systems, is characteristic of the NIT-4*f* coordination.[25,49,50] The purity of the precursor is confirmed by elemental analysis and FT-IR (absence of *ν*(-OH) stretching band, Fig. S3).

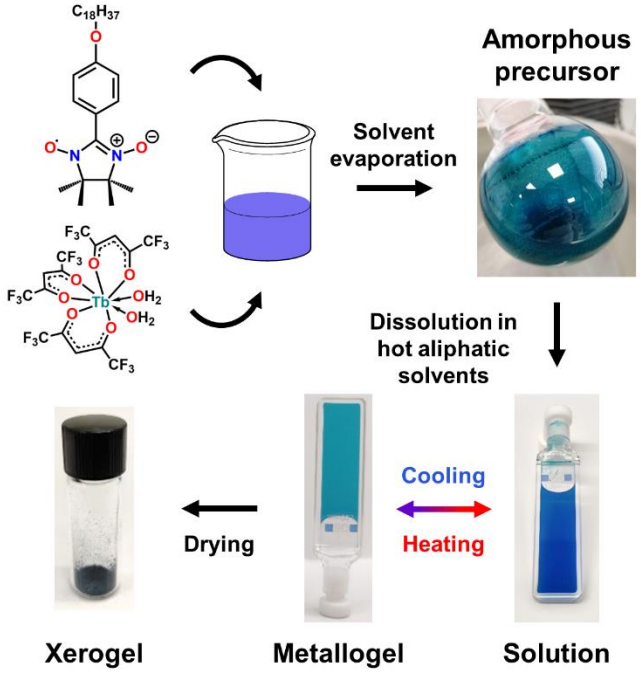

Fig. 2 Schematic procedure for the synthesis of the compounds studied in this work.

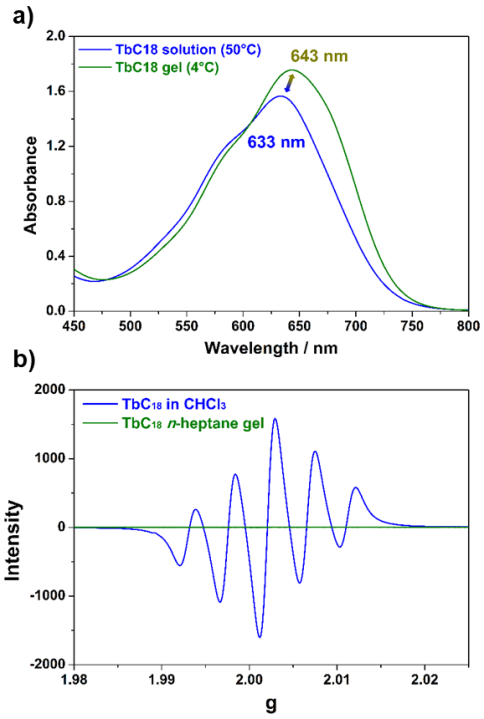

Fig. 3 (a) UV-Visible spectra of *n*-heptane TbC_{18} solution and TbC_{18} gel (C_m = 10 mg·mL^{-1}). The sol-gel transition temperature estimated by tube inversion test is 40 ± 1°C (b) Room temperature EPR spectra of a TbC_{18} precursor dissolved in $CHCl_3$ and an *n*-heptane TbC_{18} gel (C_m = 10 mg·mL^{-1}).

Metallogel formation is governed here by three main factors: *i*) coordination bondings that are responsible for the growth of chain structures *ii*) intramolecular (or intra-chain in the present case) non-covalent interactions (H-bonding, van der Waals, π-stacking) that ensure their robustness (on NIT chains, these interactions are mainly π-stacking interactions between aromatic hfac$^-$ and phenyl moieties of the NIT),[51,52] *iii*) intermolecular (or inter-chain) non-covalent interactions between functional groups that induce their supramolecular self-assembly. Additionally, the solvent plays a crucial role since it stabilizes the supramolecular edifice without competing with all these interactions.

The gelling properties of the amorphous solid TbC_{18} precursor were evaluated toward various usual solvents (Table S2): only the linear non-coordinating aliphatic solvents (*n*-hexane, *n*-heptane, *n*-octane, *n*-decane) afforded a translucent cyan TbC_{18} gel after tens of minutes (Fig. 2) with the best gelation ability attributed to the *n*-decane (C_m = 5 mg·mL^{-1}). However, the best stability and aging behavior were found for n-heptane gels (C_m = 10 mg·mL^{-1}), which can be stored for three months at 4°C with no sign of degradation. We used these gels in the following study. Notably, no gel was obtained by applying the same procedures to the unreacted $Tb(hfac)_3{\cdot}2H_2O$ and $NITPhOC_{18}$ building blocks. Consequently, $NITPhOC_{18}$ can be considered as an organogelator only when coordinated with the bridging $Tb(hfac)_3$ complex that acts as a "linking node" and "structuring agent".[26] The sol-gel transition temperature estimated by tube inversion test is 40 ± 1°C. In addition to this obvious change of viscosity, a significant color change from blue to cyan is observed during the sol-gel transition as reported in Fig. 2 and 3a. The main absorption band shifts from 633 nm for the hot blue solution to 643 nm for the cyan gel. This 10 nm hypsochromic shift is characteristic of the coordination between the $Tb(hfac)_3$ and the NIT moieties giving rise to MLCT transitions as observed on TbC_6 crystal helical chains[25] as well as on other NIT-based coordination complexes.[49,53]

To evaluate the gel quality we took advantage of the sensitivity of the nitroxide radicals toward Electron Paramagnetic Resonance (EPR) spectroscopy that has been used as spin-label to monitor the assembly and gelation dynamics of radical-based but metal-free organogelators.[54–58] Room temperature X-band EPR signals of $NITPhOC_{18}$ and TbC_{18} precursor in $CHCl_3$ solutions exhibit very clear and characteristic five-line spectra with 1:2:3:2:1 intensity ratio, g-factor, and values consistent with those found in the literature for free NIT radicals (see Fig. 3b and S4, Table S3). This indicates that de-coordination occurs when the TbC_{18} precursor is poured into a $CHCl_3$ solution. This is in contrast with the TbC_{18} gel spectrum recorded under the same experimental conditions, which is remarkably flat because of the Tb-NIT coordination that favors fast electronic relaxation as well as the increased viscosity and associated loss of mobility. Possibly, free NIT contribution can be observed only in very sensitive measuring conditions as a noisy signal indicates extremely small traces of free NIT radical (Fig. S5).

Morphology and structural model

In order to provide some insights into the supramolecular arrangement of TbC_{18} gel, small-angle X-ray spectroscopy (SAXS) measurements have been performed (Fig. 4). This technique is mainly sensitive to the electronic density contrast between the different elements of the system.

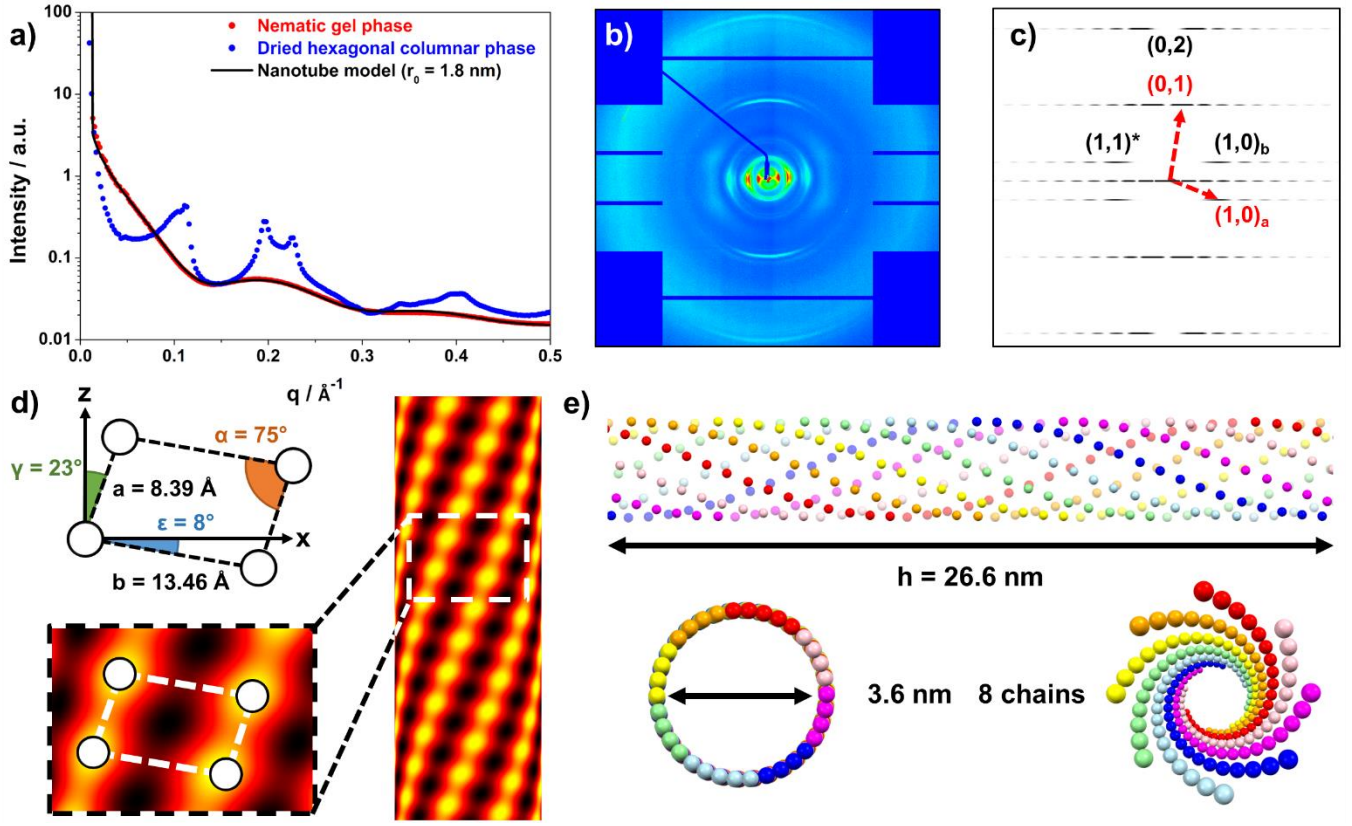

Fig. 4 (a) X-ray scattering pattern of *n*-heptane TbC_{18} gel and dried fibers (C_m = 50 mg·mL^{-1}). (b) Oriented X-ray fiber scattering image of a dried *n*-heptane TbC_{18} gel (C_m = 50 mg·mL^{-1}). (c) Simulations of diffuse scattering by Bessel functions corresponding to the Fourier transform of a 2D lattice. (d) Representation of the monoclinic unit cell and the corresponding parameters, and reconstructed 2D Patterson function, indicating the main electron density variation of the unit cell and enlarged 2D Patterson function of the resulting nanotube. (e) Representation of the supramolecular nanotube extracted from the Tb^{III} tube model of TbC_{18} gel.

In our case, it allows probing the relative spatial organization of the heavy element, i.e. the Tb^{III} ions, compared to lighter atoms such as carbon, nitrogen, or oxygen. The intensity profiles (Fig. 4a) revealed the presence of two oscillations in the low q region (q < 0.5 Å^{-1}), characteristic of a tubular organization. Indeed, for an infinite hollow tube, the intensity $I(q)$ can be described as the following model,[59] with J_0 a zeroth-order Bessel function and r_0 the radius of the tube:

$$I(q) = \frac{J_0(qr_0)^2}{q^2} \qquad \text{Eq.1}$$

The best fit (Fig. 4a) is obtained for r_0 = 1.8 nm, suggesting that the supramolecular tubes feature a diameter of $\varnothing_{gel\ Tb\text{-}Tb}$ = 3.6 nm considering the relative Tb^{III} positions. These metrics are strongly reminiscent of the supramolecular architecture also observed in the TbC_6 crystalline phase ($\varnothing_{cryst\ Tb\text{-}Tb}$ = 5.0 nm) with shorter chain derivative.[25] This first result confirms that the use of long alkyl chains in the NIT not only induces a gel-like behavior but also preserves the supramolecular nanotube organization of the chains in TbC_{18} gel. Hence, the molecular nanotubes are stable when the constraints of the crystal packing and the weak non-covalent interaction between them are softened in gel media. However, from the bulk gel sample, the nanotubes are randomly organized, and only the statistical value of the characteristic dimension, *i.e.* the diameter, can be determined.

To gain order in the gel, a concentrated *n*-heptane TbC_{18} gel sample (C_m = 50 mg·mL^{-1}) has been slowly dried to align the fibers against the capillary walls, revealing anisotropically oriented rings on SAXS scattering image (see Fig. 4b). Fiber diffraction patterns of thin nanotubes are composed of horizontal Bessel functions that give information on the 2D lattice supported by the nanotube wall.[59–61] More precisely, the indexation of the position of diffuse scattering maxima provides parameters of the elementary monoclinic unit cell of a nanotube (Fig. 4c and d), which can be seen as a folded 2D crystal lattice along the tube direction. Pattern simulation[61] (Fig. 4d) strongly suggests the following cell parameters: a = 8.39 Å, b = 13.46 Å and α = 75°, this unit cell being at γ = 23° from the

tube direction and ε = 8° from its equatorial plane. Scattering intensities can be also injected in a 2D Patterson cylindrical map[59] that stresses the tubular organization of the helical chains (Fig. 4d). 2D unit cell values are linked to Tb-Tb distances and can be unambiguously assigned to the distance between two consecutive Tb^{III} ions along the chain (parameter *a*) and between two neighboring chains (parameter *b*). The *a* parameter is almost unchanged from TbC_6 crystal tubes to gel TbC_{18} tubes. In the TbC_6 crystal, Tb-Tb distances range from 8.31 to 8.48 Å depending on the crystallographically different Tb^{III} ions. As expected, this value is averaged on the TbC_{18} gel with *a* = 8.39 Å. On the contrary, the smallest Tb-Tb interchain distance changes from TbC_6 crystal to TbC_{18} gel with an increase from 10.80 Å to *b* = 13.46 Å. This means that the geometry of each chain is almost unaffected by the crystal-to-gel change but each of them is more separated in the gel. Accordingly, this strongly suggests the persistence of the SCM behavior in the gel phase because intrachain Tb-Tb distances are preserved while interchain Tb-Tb distances are enhanced.

There are also more macroscopic differences between the two tubes in the number of chains per tube and their helical pitch length. The number of chains can be estimated by comparing *b* with the perimeter of the tube $2\pi r_0$. Tubes are made of eight chains in TbC_{18} gel instead of eleven in TbC_6 crystal. The helical pitch length is driven by the angle ε of the 2D cell with the equatorial plane. Accordingly, the pitch h of the chains is longer in the TbC_{18} gel *h* = 26.6 nm ($\varnothing_{gel\ Tb\text{-}Tb}$ = 3.6 nm and γ = 23°) than in TbC_6 crystal *h* = 19.8 nm ($\varnothing_{crist\ Tb\text{-}Tb}$ = 5.0 nm and γ = 51°). All these findings show that supramolecular nanotubes are made of less numerous and less closely packed chains in the gel than in the crystal.

Using all the extracted parameters, it is then possible to build a 3D structural model of TbC_{18} gel using helices parametric equations. This model can be exploited as an atom coordinate file (Table S4) and easily visualized (Fig. 4e, S6-S8 and procedure in SI), making the understanding of this supramolecular arrangement way easier.

Magnetic properties

Static magnetic properties have been measured on frozen fresh *n*-heptane TbC_{18} gel and ground powder of TbC_{18} xerogel under a static field (H_{DC} = 1000 Oe) (Fig. 5a and S9). High temperature values of $\chi_M T$ are $\chi_M T_{(150K,\ gel)}$ = 12.25 emu·K·mol^{-1} and $\chi_M T_{(300K,\ xerogel)}$ = 12.52 emu·K·mol^{-1}, close to the theoretical $\chi_M T_{(300K)}$ = 12.19 emu·K·mol^{-1} for a free Tb^{III} ion (J = 6, g_J = 3/2) and an uncoupled radical (S = 1/2, g_S = 2). By decreasing the temperature, these values stay constant and then increase exponentially below 100 K to reach maxima of $\chi_M T_{(gel)}$ = 21.73 emu·K·mol^{-1} at 4.5 K and $\chi_M T_{(xerogel)}$ = 22.29 emu·K·mol^{-1} at 5.5 K. At lower T a sharp decrease is visible due to saturation effect as highlighted by $\chi_M T$ values reconstructed from ac dynamic magnetic measurements (inset Fig. 5a). Field dependence of the magnetization exhibits an abrupt rise starting at the lowest fields and quickly reaching saturation values at 50 KOe of $M_{(sat\ gel)}$ = 5.06 μ_B and $M_{(sat\ xerogel)}$ = 5.07 μ_B respectively, slightly below

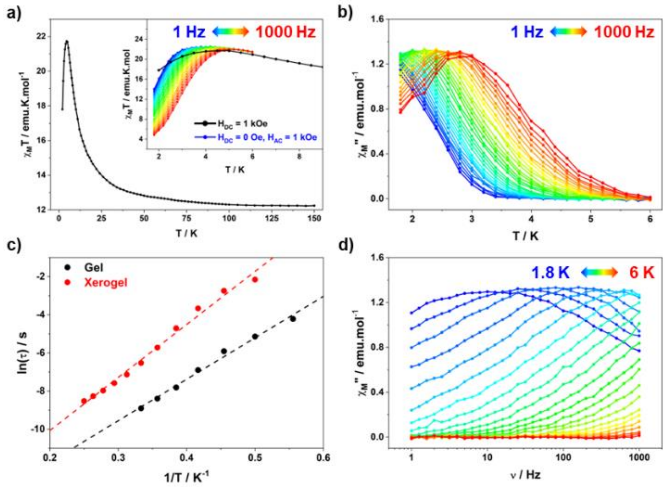

Fig. 5. (a) Temperature dependence of $\chi_M T$ product for *n*-heptane TbC_{18} gel (C_m = 10 mg·mL^{-1}), in inset a zoom in the low-temperature region with the $\chi_M T$ product reconstructed from AC measurements at different frequencies. (b) Temperature dependency of the out-of-phase (χ_M'') susceptibility of *n*-heptane TbC_{18} gel (C_m = 10 mg·mL^{-1}) at different frequencies. (c) Arrhenius plot of the extracted relaxation times of *n*-heptane TbC_{18} gel (C_m = 10 mg·mL^{-1}) and TbC_{18} xerogel, together with the corresponding fits as dashed lines. (d) Frequency dependency of the out-of-phase (χ_M'') susceptibility of *n*-heptane TbC_{18} gel (C_m = 10 mg·mL^{-1}) at different temperatures.

the theoretical value of 5.5 μ_B (Fig. S10). All these magnetic features are in line with the onset of a magnetic correlation phenomenon at low temperature along the chains, a signature of an SCM behavior. Accordingly, the exponential divergence of the $\chi_M T$ product can be linked to Δ_ξ, the correlation energy required to create a domain wall, as $\chi_M T = C_{eff}.\exp(\Delta_\xi/k_B T)$. These values are respectively $\Delta_{\xi(gel)}/k_B$ = 4.26 ± 0.02 K (R^2 = 0.9992) for TbC_{18} gel, and $\Delta_{\xi(xero)}/k_B$ = 5.39 ± 0.03 K (R^2 = 0.9988) for TbC_{18} xerogel (Fig. S11) and are in line with the ones observed on the TbC_6 crystal.[25]

Dynamic magnetic measurements under zero external field further confirm these findings. In-phase (χ_M') and out-of-phase (χ_M'') susceptibilities exhibit an unambiguous temperature dependence below 6 K, synonym of slow relaxation of the magnetization (Fig. 5b, d and S12-S13). The corresponding relaxation times τ were extracted using a generalised Debye model and fitted according to an Arrhenius law $\tau = \tau_0.\exp(\Delta_{eff}/k_B T)$, where Δ_{eff} is the effective energy barrier and τ_0 the characteristic relaxation time: for TbC_{18} gel, the fitted values are Δ_{gel}/k_B = 21.1 ± 0.9 K and τ_{gel} = (1.04 ± 0.53) × 10^{-7} s (R^2 = 0.9889) while the TbC_{18} xerogel is characterised by Δ_{xero}/k_B = 27.7 ± 0.9 K and τ_{xero} = (1.65 ± 0.68) × 10^{-7} s (R^2 = 0.9882) (Table S5-S6). These values as well as the in-field behavior (Fig. S14) are in line with the ones extracted on TbC_6 crystal.

The magnetic slow relaxations observed on TbC_{18} gel and TbC_{18} xerogel are slow enough to induce an opening of a magnetic hysteresis loop at T = 0.5 K (Fig. 6) in our operating conditions of magnetic field sweep rate of 15.5 Oe·s^{-1}. It is worth noting that contrary to what is observed on most 4*f*-based SMMs, SCMs hysteresis are open in zero-field, the molecules acting as molecular magnets with a non-null remnant magnetization (M_R) and an associated coercive field (H_C).

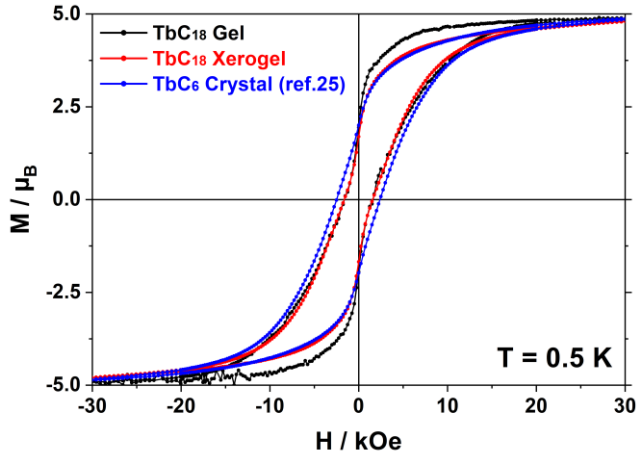

Fig. 6. Magnetic hysteresis curves of *n*-heptane TbC_{18} gel (black dots, C_m = 10 mg·mL^{-1}), TbC_{18} xerogel (red dots) and TbC_6 crystal (blue dots) at 0.5 K with magnetic field sweep rate of 15.5 Oe·s^{-1}.

Hysteresis shapes and associated magnetic metrics are very close for both TbC_{18} gel and TbC_{18} xerogel and was strongly reminiscent to what observed on the TbC_6 crystal (Table 1) with $H_{C\ (TbC18\ gel)}$ = 1610 Oe, $H_{C\ (TbC18\ xerogel)}$ = 1600 Oe, $M_{R\ (TbC18\ gel)}$ = 1.94 μ_B and $M_{R\ (TbC18\ xerogel)}$ = 1.71 μ_B. As expected, this highlights that the substitution of the NIT radical from a hexyl to an octadecyl tail weakly impacts the magnetic properties of the corresponding SCMs. Additionally, the very weak difference between gel and xerogel magnetic behavior shows that SCM properties are preserved upon gel drying. They are intrinsic properties of the molecular chains whatever the crystal packing or the state of matter they are involved in. This is a strong asset to transform these compounds into magnetic materials. To the best of our knowledge, this is the first time that a magnetic hysteresis loop with a magnetic slow relaxation of molecular origin is reported in metallogels, expanding so the family of molecular magnetic materials.

Surface deposition

To confirm the nanotube dimensions estimated by SAXS measurements, and to pave the road toward an SCM-based magnetic layer, thin films of TbC_{18} gel were obtained by optimizing a deposition protocol (see SI for details) based on the spin-coating of drop-casted hot solutions on silicon wafer and a rapid temperature quenching. These conditions were mandatorily required to achieve a controlled deposition of nanotubes as confirmed by AFM measurements. In particular, at a concentration of C_m = 1.7 mg·mL^{-1}, isolated and randomly oriented fibers were successfully observed (Fig. 7a). Line profile analysis (Fig. 7b) and histogram analysis (Fig. 7c) confirmed the presence of individual nanotubes. In particular, the latter has been performed considering the entire image and operated after a line-by-line background alignment (see SI) revealing unambiguously the presence of a multimodal distribution accounting for the silicon substrate (artificially centered at H_0 = 0 nm), the presence of the main component attributable to the single fibers heights (H_1 = 4.8 ± 1.1 nm) in contact with the substrate and a third term assigned to the second layer of fibers (H_2 = 9.1 ± 1.5 nm) is highlighted here.

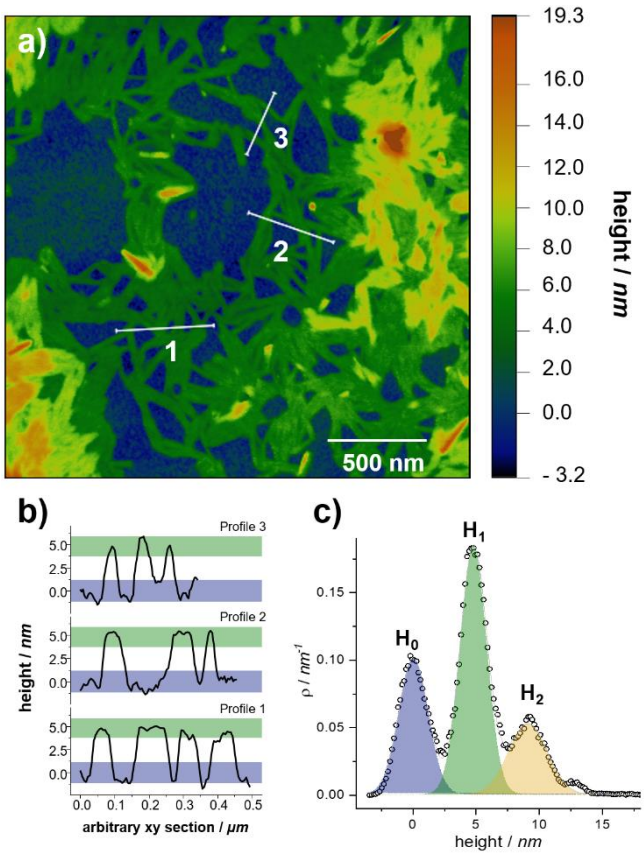

Fig. 7. (a) AFM image of a *n*-heptane TbC_{18} gel (C_m = 1.7 mg·mL^{-1}) deposited on silicon surface. (b) Relative height profiles of individual nanotubes determined from image a). (c) Histogram analysis of image a) and the relative deconvolution analysis highlighting the presence of individual nanotubes.

Thus, even though the width of fibers cannot be directly evaluated because of the convolution of the AFM tip, the detected height of fibers results in good agreement with the diameter of the tubular objects determined by SAXS measurements thus suggesting that we successfully deposited isolated SCMs on surface.

Table 1 Summary of the principal magnetic values for the *n*-heptane TbC_{18} gel (C_m = 10 mg·mL^{-1}), TbC_{18} xerogel and TbC_6 crystal.[25]

	TbC6 crystal[25]	TbC18	
		Gel	Xerogel
Δ_ξ / k_B (K)	5.16 ± 0.03	4.26 ± 0.02	5.39 ± 0.03
Δ_{eff}/k_B (K) τ_0 (s)	Infinite regime: 29.6 ± 0.5 (3.4 ± 0.5) × 10^{-8} Finite regime: 25.5 ± 0.2 (2.4 ± 0.3) × 10^{-7} Single regime: 28.8 ± 0.1 (4.4 ± 0.6) × 10^{-8}	21.1 ± 0.9 (1.04 ± 0.53) × 10^{-7}	27.7 ± 0.9 1.65 ± 0.68 × 10^{-7}
α (at 1.8 K)	0.612 ± 0.02	0.675 ± 0.003	0.611 ± 0.010
H_C (Oe)	2400	1610	1600
M_R (μ_B / %M_{sat})	2.09 / 38 %	1.94 / 39 %	1.71 / 34 %

a) Arrhenius plot can be fitted with reasonable error margin considering either finite- and infinite-size regime or a single relaxation regime. For the gel, only a single regime can be reasonably provided.

Conclusions

Here we demonstrated that, by increasing the size of the aliphatic tail of the bridging NIT ligand is possible to obtain a stable SCM-based metallogel. SAXS and fiber diffraction studies revealed that the nanotubular structure made of woven helical chains observed in the genuine crystalline phase is preserved in the gel. Precise metrics of the helical nanotubes have been obtained and strong analogy between the crystal and the metallogel phase is observed by a detailed three-dimensional model. This approach is likely to be used on any type of molecular nanotubes either made of SCM or not.

The metallogel approach is efficient in stabilizing the molecular structure responsible for the SCM behavior as shown on gels and xerogels magnetic measurements where SCM signature and zero-field opened magnetic hysteresis are observed. Furthermore, the stable supramolecular architecture allowed to optimize a deposition protocol for the deposition on silicon surface of individual nanotubes as revealed by an AFM analysis. This study opens novel perspectives for the use of single-chain magnets at the nanoscale that may be used now as a novel building block for the development of novel architectures for data storage and eventually for spintronics. Finally, the metallogel approach could be tested on any molecular material (magnetic or not) whose chemical stability, or topology (such as an infinite polymeric structure) are a drawback for its surface deposition.

Author Contributions

This experiment was designed by K.B. and M.M. F.H. performed the synthesis and the characterizations of the gel. F.A. run the SAXS measurements and structural parameters determination, and F.H. have built the 3D model. F.H. and T.G. and have performed the EPR and magnetic measurements. F.H. and M.M. realized the AFM study. The manuscript was written through contributions of all authors. All authors have given approval to the final version of the manuscript.

Conflicts of interest

There are no conflicts to declare.

Acknowledgements

This work was supported by the French ministry of high education and research (MESRI), Region Bretagne, Rennes Metropole, INSA PPI program, CNRS via Florennes PICS Program. The authors acknowledge M. Dallon (CDIFX) for crystal structure refinement, K.B. acknowledges Institut Universitaire de France. M.M. and G.C. acknowledge the Italian MIUR, through the Project "Dipartimenti di Eccellenza 2018-2022 (ref. no. B96C1700020008) and Fondazione Cassa di Risparmio di Firenze (Project SPINE-2 2020.1634) for the financial support. Surface depositions have been carried out at the surface science laboratories of the MatchLab Interdepartmental Research Unit, University of Florence.

References

1 B. Sieklucka and D. Pinkowicz, Eds., *Molecular magnetic materials: concepts and applications*, Wiley-VCH Verlag GmbH & Co. KGaA, Weinheim, 2017.
2 D. Reinsel, J. Gantz and J. Rydning, *The Digitization of the World from Edge to Core*, IDC, USA, 2018.
3 *Digitalization and Energy*, IEA, 2017.
4 D. Gatteschi, R. Sessoli and J. Villain, *Molecular Nanomagnets*, Oxford University Press, 2006.
5 D. A. Thompson and J. S. Best, *IBM Journal of Research and Development*, 2000, **44**, 311–322.
6 A. J. Heinrich, W. D. Oliver, L. M. K. Vandersypen, A. Ardavan, R. Sessoli, D. Loss, A. B. Jayich, J. Fernandez-Rossier, A. Laucht and A. Morello, *Nat. Nanotechnol.*, 2021, **16**, 1318–1329.
7 C. Benelli and D. Gatteschi, *Introduction to molecular magnetism: from transition metals to lanthanides*, Wiley-VCH, Weinheim, 2015.
8 J. Ferrando-Soria, J. Vallejo, M. Castellano, J. Martínez-Lillo, E. Pardo, J. Cano, I. Castro, F. Lloret, R. Ruiz-García and M. Julve, *Coord. Chem. Rev.*, 2017, **339**, 17–103.
9 A. Cornia and M. Mannini, in *Molecular Nanomagnets and Related Phenomena*, ed. S. Gao, Springer Berlin Heidelberg, Berlin, Heidelberg, 2014, vol. 164, pp. 293–330.
10 R. J. Holmberg and M. Murugesu, *J. Mater. Chem. C*, 2015, **3**, 11986–11998.
11 F. Paschke, T. Birk, V. Enenkel, F. Liu, V. Romankov, J. Dreiser, A. A. Popov and M. Fonin, *Adv. Mater.*, 2021, 2102844.
12 A. Cornia, M. Mannini, R. Sessoli and D. Gatteschi, *Eur. J. Inorg. Chem.*, 2019, **2019**, 552–568.
13 F. Donati, S. Rusponi, S. Stepanow, C. Wackerlin, A. Singha, L. Persichetti, R. Baltic, K. Diller, F. Patthey, E. Fernandes, J. Dreiser, Z. Sljivancanin, K. Kummer, C. Nistor, P. Gambardella and H. Brune, *Science*, 2016, **352**, 318–321.
14 C. A. P. Goodwin, F. Ortu, D. Reta, N. F. Chilton and D. P. Mills, *Nature*, 2017, **548**, 439–442.
15 F.-S. Guo, B. M. Day, Y.-C. Chen, M.-L. Tong, A. Mansikkamäki and R. A. Layfield, *Science*, 2018, **362**, 1400–1403.
16 C. Sangregorio, T. Ohm, C. Paulsen, R. Sessoli and D. Gatteschi, *Phys. Rev. Lett.*, 1997, **78**, 4645–4648.

17 C. Coulon, H. Miyasaka and R. Clérac, in *Single-Molecule Magnets and Related Phenomena*, ed. R. Winpenny, Springer Berlin Heidelberg, Berlin, Heidelberg, 2006, vol. 122, pp. 163–206.
18 C. Coulon, R. Clérac, L. Lecren, W. Wernsdorfer and H. Miyasaka, *Phys. Rev. B*, 2004, **69**, 132408.
19 D. Luneau, *Eur. J. Inorg. Chem.*, 2020, **2020**, 597–604.
20 M. G. F. Vaz and M. Andruh, *Coord. Chem. Rev.,* 2021, **427**, 213611.
21 L. Bogani, A. Vindigni, R. Sessoli and D. Gatteschi, *J. Mater. Chem.*, 2008, **18**, 4750–4758.
22 D. Olea, S. S. Alexandre, P. Amo-Ochoa, A. Guijarro, F. de Jesús, J. M. Soler, P. J. de Pablo, F. Zamora and J. Gómez-Herrero, *Adv. Mater.*, 2005, **17**, 1761–1765.
23 R. Mas-Ballesté, J. Gómez-Herrero and F. Zamora, *Chem. Soc. Rev.*, 2010, **39**, 4220.
24 M. Castellano, J. Ferrando-Soria, N. Moliner, J. Cano, M. Julve and F. Lloret, *J. Coord. Chem.*, 2018, **71**, 725–736.
25 F. Houard, Q. Evrard, G. Calvez, Y. Suffren, C. Daiguebonne, O. Guillou, F. Gendron, B. Le Guennic, T. Guizouarn, V. Dorcet, M. Mannini and K. Bernot, *Angew. Chem. Int. Ed.*, 2020, **59**, 780–784.
26 F. Fages, *Angew. Chem. Int. Ed.*, 2006, **45**, 1680–1682.
27 A. Y.-Y. Tam and V. W.-W. Yam, *Chem. Soc. Rev.*, 2013, **42**, 1540.
28 M.-O. M. Piepenbrock, G. O. Lloyd, N. Clarke and J. W. Steed, *Chem. Rev.*, 2010, **110**, 1960–2004.
29 R. Weeber, M. Hermes, A. M. Schmidt and C. Holm, *J. Phys. Condens. Matter*, 2018, **30**, 063002.
30 P. R. A. Chivers and D. K. Smith, *Nat Rev Mater*, 2019, **4**, 463–478.
31 C. D. Jones and J. W. Steed, *Chem. Soc. Rev.*, 2016, **45**, 6546–6596.
32 P. Sutar and T. K. Maji, *Inorg. Chem.*, 2017, **56**, 9417–9425.
33 P. Chen, Q. Li, S. Grindy and N. Holten-Andersen, *J. Am. Chem. Soc.*, 2015, **137**, 11590–11593.
34 S. Dhibar, A. Dey, S. Majumdar, A. Dey, P. P. Ray and B. Dey, *Ind. Eng. Chem. Res.*, 2020, **59**, 5466–5473.
35 J. Y. R. Silva, L. L. da Luz, F. G. M. Mauricio, I. B. Vasconcelos Alves, J. N. de S. Ferro, E. Barreto, I. T. Weber, W. M. de Azevedo and S. A. Júnior, *ACS Appl. Mater. Interfaces*, 2017, **9**, 16458–16465.
36 S. Dhibar, A. Dey, S. Majumdar, D. Ghosh, A. Mandal, P. P. Ray and B. Dey, *Dalton Trans.*, 2018, **47**, 17412–17420.
37 X.-Q. Wang, W. Wang, G.-Q. Yin, Y.-X. Wang, C.-W. Zhang, J.-M. Shi, Y. Yu and H.-B. Yang, *Chem. Commun.*, 2015, **51**, 16813–16816.
38 C. Kim, K. Y. Kim, J. H. Lee, J. Ahn, K. Sakurai, S. S. Lee and J. H. Jung, *ACS Appl. Mater. Interfaces*, 2017, **9**, 3799–3807.
39 M. Xue, Y. Lü, Q. Sun, K. Liu, Z. Liu and P. Sun, *Crystal Growth & Design*, 2015, **15**, 5360–5367.
40 S. Tang and B. D. Olsen, *Macromolecules*, 2016, **49**, 9163–9175.
41 L. Wang, H. Xu, J. Gao, J. Yao and Q. Zhang, *Coord. Chem. Rev*, 2019, **398**, 213016.
42 I. A. Gural'skiy, V. A. Reshetnikov, A. Szebesczyk, E. Gumienna-Kontecka, A. I. Marynin, S. I. Shylin, V. Ksenofontov and I. O. Fritsky, *J. Mater. Chem. C*, 2015, **3**, 4737–4741.
43 O. Roubeau, A. Colin, V. Schmitt and R. Clérac, *Angew. Chem. Int. Ed.*, 2004, **43**, 3283–3286.
44 T. Fujigaya, D.-L. Jiang and T. Aida, *Chem. Asian J.*, 2007, **2**, 106–113.
45 P. Grondin, O. Roubeau, M. Castro, H. Saadaoui, A. Colin and R. Clérac, *Langmuir*, 2010, **26**, 5184–5195.
46 Y. Wu, Y. Hirai, Y. Tsunobuchi, H. Tokoro, H. Eimura, M. Yoshio, S. Ohkoshi and T. Kato, *Chem. Sci.*, 2012, **3**, 3007.
47 K. Mori, R. Eguchi, S. Karasawa and N. Koga, *Inorg. Chem. Front.*, 2015, **2**, 917–926.
48 E. F. Ullman, J. H. Osiecki, D. G. B. Boocock and R. Darcy, *J. Am. Chem. Soc.*, 1972, **94**, 7049–7059.
49 A. Lannes, M. Intissar, Y. Suffren, C. Reber and D. Luneau, *Inorg. Chem.*, 2014, **53**, 9548–9560.
50 F. Houard, F. Gendron, Y. Suffren, T. Guizouarn, V. Dorcet, G. Calvez, C. Daiguebonne, O. Guillou, B. Le Guennic, M. Mannini and K. Bernot, *Chem. Sci.*, 2021, **12**, 10613–10621.
51 A. Caneschi, D. Gatteschi, N. Lalioti, C. Sangregorio and R. Sessoli, *J. Chem. Soc., Dalton Trans.*, 2000, 3907–3912.
52 L. Bogani, C. Sangregorio, R. Sessoli and D. Gatteschi, *Angew. Chem. Int. Ed.*, 2005, **44**, 5817–5821.
53 R. Beaulac, G. Bussière, C. Reber, C. Lescop and D. Luneau, *New J. Chem.*, 2003, **27**, 1200–1206.
54 R. G. Weiss and P. Terech, Eds., *Molecular gels: materials with self-assembled fibrillar networks*, Springer, Dordrecht, 2006.
55 M. Kveder, M. Andreis, J. Makarević, M. Jokić and B. Rakvin, *Chem. Phys. Lett.*, 2006, **420**, 443–447.
56 P. Terech, *J. Colloid Interface Sci*, 1985, **107**, 244–255.
57 P. Terech, R. Ramasseul and F. Volino, *J. Colloid Interface Sci.*, 1983, **91**, 280–282.
58 M. Mannini, S. Cicchi, D. Berti, A. Caneschi, A. Brandi, L. Lascialfari and L. Sorace, *ChemPlusChem*, 2013, **78**, 149–156.
59 C. Valery, M. Paternostre, B. Robert, T. Gulik-Krzywicki, T. Narayanan, J.-C. Dedieu, G. Keller, M.-L. Torres, R. Cherif-Cheikh, P. Calvo and F. Artzner, *PNAS*, 2003, **100**, 10258–10262.
60 C. Tarabout, S. Roux, F. Gobeaux, N. Fay, E. Pouget, C. Meriadec, M. Ligeti, D. Thomas, M. IJsselstijn, F. Besselievre, D.-A. Buisson, J.-M. Verbavatz, M. Petitjean, C. Valery, L. Perrin, B. Rousseau, F. Artzner, M. Paternostre and J.-C. Cintrat, *PNAS*, 2011, **108**, 7679–7684.
61 C. Valéry, S. Deville-Foillard, C. Lefebvre, N. Taberner, P. Legrand, F. Meneau, C. Meriadec, C. Delvaux, T. Bizien, E. Kasotakis, C. Lopez-Iglesias, A. Gall, S. Bressanelli, M.-H. Le Du, M. Paternostre and F. Artzner, *Nat. Commun*, 2015, **6**, 7771.

